JOURNAL of
MATERIALS and MECHATRONICS:A

e-ISSN 2717-8811
JournalMM, 2024, 5(1), 14-35
https://doi.org/10.55546/jmm.1447858

Araştırma Makalesi / Research Article

Effect of Thermo-Reactive Diffusion Coatings on Microstructure and Wear Behavior of Powder Metallurgy Steel Cutting Inserts

Talat TURAN[1], Ali GÜNEN[2], Erdoğan KANCA[3*]

[1]Iskenderun Technical University, Faculty of Engineering and Natural Sciences, Department of Mechanical Engineering, Hatay, Turkey,
ORCID ID: https://orcid.org/0009-0000-4693-7163, turantalat46@gmail.com
[2] Iskenderun Technical University, Faculty of Engineering and Natural Sciences, Department of Mechanical Engineering, Hatay, Turkey,
ORCID ID: https://orcid.org/0000-0002-4101-9520, ali.gunen@iste.edu.tr
[3*]Iskenderun Technical University, Faculty of Engineering and Natural Sciences, Department of Mechanical Engineering, Hatay, Turkey,
ORCID ID: https://orcid.org/0000-0002-7997-9631, erdogan.kanca@iste.edu.tr

Geliş/ Received: 07.03.2024**;** **Revize/Revised:** 05.04.2024 **Kabul / Accepted:** 13.04.2024

ABSTRACT: In this study, powder metallurgy-produced 1.337 steel (PMS 1.3377) was subjected to boronizing, titanizing, and vanadinizing processes at 950 °C for 2 hours. The influence of boride and carbide coatings formed on the surface of PMS 1.3377 on the microstructure of these steels and their wear behaviors at room temperature and 500 °C were investigated. Characterization of the formed coating layers was carried out through Scanning Electron Microscopy (SEM-EDS), X-ray Diffraction (XRD), microhardness, and wear testing. Wear tests considering the cutting tool turning, milling, and drilling applications of PMS 1.3377 were conducted at room temperature and 500 °C in ambient air with a 10 N load and a 250 m sliding distance against an Al_2O_3 ball. Metallographic studies showed that coating layers with thicknesses of 98±2.1, 11±0.5, 13.5±0.6 µm and hardness of 2566±125 HV0.1, 2037±104 HV0.1, and 1800±197 were obtained by boronizing, titanizing and vanadinizing processes, respectively. The dominant phase structures in the obtained coatings were determined to be FeB, TiC, and VC for boronizing, titanizing, and vanadinizing, respectively. Due to the high hardness of boride and carbide phases and their ability to form more stable oxide layers during wear, the coated samples exhibited lower friction coefficients and lower wear volume losses. While untreated PMS 1.3377 experienced delamination and oxidation wear mechanisms at room temperature, the wear mechanism at 500 °C transformed into adhesive and oxidation wear. On the other hand, in the coated samples, the wear mechanism was found to occur as adhesive, oxidative, and delamination at both room temperature and 500 °C.

Keywords: Powder metallurgy, Thermo-reactive diffusion technique, Hardness, Friction, Wear.

*Sorumlu yazar / Corresponding author: erdogan.kanca@iste.edu.tr
Bu makaleye atıf yapmak için /To cite this article

Turan, T., Günen, A., Kanca, E. (2024). Effect of Thermo-Reactive Diffusion Coatings on Microstructure and Wear Behavior of Powder Metallurgy Steel Cutting Inserts. Journal of Materials and Mechatronics: A (JournalMM), 5(1), 14-35.

1. INTRODUCTION

Cutting inserts are essential components in various machining operations like turning, milling, and drilling, where they are used to shape workpieces accurately and efficiently (König et al., 1984; Gürbüz et al., 2020; Hasçelik and Aslantaş 2021). Powder metallurgy (PM) is a versatile and cost-effective method for producing cutting edges with tailored properties for various machining applications (Angelo et al., 2022; Aras et al. 2022). By utilizing metal powders, PM offers a wide range of material composition choices that may not be achievable through conventional methods (Erden et al., 2021). The production of cutting tools using the PM technique involves the development of composite materials through the consolidation of metal powders (Rizzo et al., 2020). This process allows for the creation of cutting edges with enhanced properties such as wear resistance, hardness, and dimensional stability. Studies have shown that PM is energetically efficient and economically feasible for producing both simple and complex cutting edge designs to meet specific dimensional requirements (Şap et al., 2021; Nayak et al. 2022; Gökmen, 2023).

Furthermore, advancements in PM technology have enabled the production of cutting tools with improved machinability, microstructural properties, and corrosion resistance. By optimizing sintering parameters and material compositions, PM offers a viable route for fabricating cutting tools with superior mechanical and corrosion properties (Nayak et al., 2022; Sathish et al., 2021). The unique advantages of PM, such as near-net shape forming capabilities and freedom in material composition selection, make it an attractive method for producing cutting edges with tailored properties (Angelo et al., 2022; Somunkıran et al., 2022). Researchers have also explored the impact of PM on the tribological behavior and machinability of cutting edges, highlighting the potential for enhancing cutting performance through PM-synthesized materials (Aras et al., 2022; Liu et al., 2023).

Although cutting inserts produced by powder metallurgy are used in many machinability applications, the corrosive working conditions to which these inserts are exposed have revealed the need for studies to increase the lifespan of these inserts. For this purpose, alloying these metal tips or making surface modifications as a secondary process are among the main topics studied (Rizzo et al., 2020; Erden et al., 2021; Vijaya Kumar and Velmurugan 2022). Although these methods have advantages and disadvantages compared to each other, the fact that cutting inserts end their useful life due to surface damage has made the improvement of these materials with surface modifications often a cost-effective method. Recent advancements in cutting edge coatings have been focused on improving tool performance and sustainability. Strategies such as applying advanced coatings like TiAlN, AlCrN, and TiCN on cutting inserts have been explored to enhance tool wear resistance, reduce cutting forces, and improve surface quality during machining processes (Daicu et al., 2017; Mathivanan et al., 2021). These coatings have demonstrated potential in extending tool life and enhancing machining efficiency, particularly when working with challenging materials such as super duplex stainless steels and nickel-based superalloys (Khan & Gupta, 2020).

The utilization of 1.3377 cutting tools produced by the powder metallurgy method offers a promising approach for developing cutting edges with enhanced properties tailored to meet the demands of modern machining processes. Powder metallurgy enables the production of cutting tools with superior wear resistance, hardness, and dimensional stability through the consolidation of metal powders. This method allows for the creation of cutting tools with improved mechanical properties and corrosion resistance, contributing to enhanced machining efficiency and prolonged tool longevity (Fang et al., 2017; Gevorkyan et al., 2021).

Boronizing, titanizing, and vanadinizing coatings produced by thermo-reactive methods offer significant advantages when applied to materials produced by the powder metallurgy and casting methods (Arai 2015; Kayalı and Yalçın 2020; Ghadi et al., 2023; Turgut and Günen 2020; Günen et al., 2023). Boriding coatings enhance wear resistance and hardness, crucial for materials used in cutting tools, thereby extending tool life and improving machining efficiency (Günen et al. 2016). Titanizing coatings provide enhanced mechanical properties and corrosion resistance, ideal for materials requiring durability and protection against environmental factors (Pashechko et al., 2020). Vanadinizing coatings improve adhesion properties, making them valuable for applications where strong bonding is essential (Dement et al., 2018).

The thermo-chemical methods used to produce these coatings allow for precise control over the coating process, ensuring that the coatings are tailored to the specific properties required for materials produced by powder metallurgy. Boriding, titanizing, and vanadinizing coatings offer advantages such as improved wear resistance, enhanced mechanical properties, and increased corrosion resistance, making them valuable for enhancing the performance and longevity of materials produced by powder metallurgy (Duran et al., 2021; Calik et al., 2021; Pashechko et al., 2020; Dement et al., 2018). Additionally, the ability to combine these coatings with powder metallurgy materials further enhances their benefits, offering a comprehensive solution for improving material properties and performance (Çaligülü et al., 2021).

In this study, it was aimed to improve the surface hardness and wear resistance of PMS 1.3377 cutting tools produced by the powder metallurgy method by applying boriding, titanizing and vanadinizing. In this context, PMS 1.3377 was subjected to boriding, titanizing and vanadinizing processes at 950 °C for 2 hours, creating boride or carbide phases on the surface. The influence of boride and carbide coatings formed on the surface of PMS 1.3377 on the microstructure of these steels and their wear behaviors at room temperature and 500 °C were investigated.

2. MATERIALS AND METHODS

2.1 Materials

The powder metallurgy-produced 1.3377 steel (1.3377 PMS) used in this study was purchased from KORKMAZ ÇELİK AŞ (Istanbul, Turkey). This powder metallurgy steel is widely used in turning, milling, CNC cutting and drilling applications. The chemical composition of the 1.3377 powder metallurgy steel, obtained from the technical documentation provided by the supplier company, is presented in Table 1.

Table 1. Chemical composition of 1.3377PMS.

Material	C	Cr	Mo	W	Co	V	Fe and impurities
1.3377	1.50	4.0	2.5	2.5	-	4.0	Balance

2.2 Determination of Used Powders and Coating Methods

Based on the satisfactory results obtained in TRD studies in the literature in improving the wear resistance of high carbon content steels, it was decided to use B_4C, Fe-Ti and Fe-V powders as coating powders (Kurt et al., 2018; Turgut and Günen 2020; Günen et al., 2020). $NaBF_4$ was used as an activator for boronizing, while NH_4CI activator was used for titanizing and vanadinizing. Ferro vanadium powder consists of 82% V, 1.5% Al, 0.25% C, 0.03% P, and 0.03% S, with a density of 6.4 g/cm³ and particle size <91 μm. B_4C powder is composed of 95% B_4C, with a density of 2.52

g/cm³ and a particle size <25 μm. Ferro titanium powder contains 73% Ti, 4% Al, 0.5% C, 0.25% Si, 0.02% S, and the balance is Fe, with a density of 3.95 g/cm³ and a particle size <43 μm. The weight percentages of the powders used in the coating processes were determined based on previous studies in the literature (Kurt et al., 2018; Turgut and Günen, 2020; Günen et al., 2020). Due to the necessity for a more economical industrial-scale coating process, a decision was made to use a cost-effective and high-quality ferroalloy instead of pure powders. Table 2 presents the powders used for the three coatings and their weight ratios.

Table 2. Weight percentages of powders used in the coating processes.

TRD processing	B_4C	$NaBF_4$	Fe-Ti	Fe-V	Al_2O_3	NH_4Cl
Boronizing	90	10	-	-	-	-
Titanizing	-	-	45	-	45	10
Vanadinizing	-	-	-	45	45	10

2.3 Preparation of Samples for Coating Process

Prior to the coating process, samples obtained from the company were acquired with rough dimensions of 20 × 30 × 1000 mm³. Precise machining techniques were employed on the sample to bring it to its final dimensions. Machining processes included milling, drilling, and cutting techniques. The surface of the sample was gradually polished using 1200-grit SiC sand paper through precision sanding. Considering that three different coating processes would be applied to samples measuring 19 × 19 × 8 mm³, three samples were manufactured for each type of coating. For optical, SEM, EDS, XRD tests, and analyses, samples measuring 10 × 10 × 10 mm³ were prepared from these larger samples. The prepared sample for the coating process is illustrated in Figure 1.

Due to the high temperatures involved in the coating process, and considering the affinity of the ferro powder components used to oxygen, a 20 mm-thick layer of Al_2O_3 powder was applied to the top surface of the powders. This layer was sealed with an airtight cover to prevent contact with oxygen. The coating steps are shown in Figure 1. Coating processes were carried out by placing the samples embedded in coating powders within air-tight steel crucibles in an atmosphere-controlled furnace at 950 ºC for 2 hours. Subsequently, the crucibles were left to cool in an open-air environment as stated in the previous study (Günen et al. 2022b).

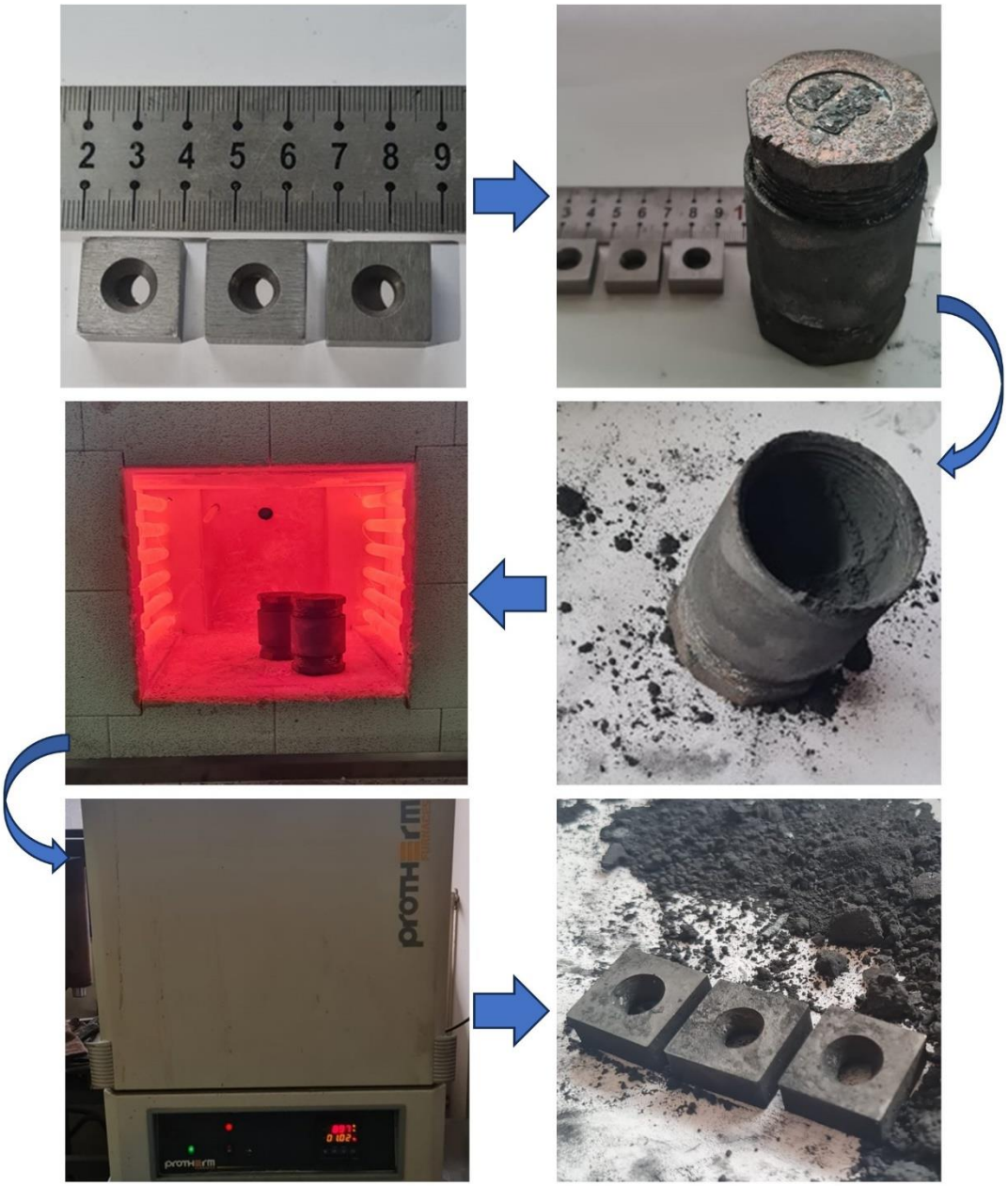

Figure 1. Representation of coating process steps.

2.4 Metallographic Studies

The coated specimens were precision-cut into dimensions of 10×10×5 mm³ using a precision cutter for microstructural analysis, hardness testing, corrosion analysis, wear testing, and XRD analysis. Following the cutting process, the specimens designated for microstructure examinations were embedded in hot bakelite, and subsequent polishing steps with SiC sandpaper ranging from 320 to 2500 grit were performed. Subsequently, precise polishing was achieved using 3 and 1-micron diamond solutions to obtain a mirror-like smooth surface. For a clearer observation of grain boundaries, the specimens were etched with a 3% nital solution for 3-6 seconds.

The Thermo Fisher Scientific Apreo S SEM device was employed for SEM analysis. In addition to SEM examinations, EDS and X-ray methods were utilized to identify carbides and phases formed in coating layers and intermediate regions. For XRD analysis, a Malvern Panalytical EMPYREAN device was used, applying 30mA and 40kV current and voltage values with Cu-K-α radiation at room

temperature. Diffraction patterns were recorded in the angular range of 10 to 90° at a fixed grazing angle (0.8°), obtaining a strong signal at a speed of 2°/minute and a step size of 0.02°.

Following the acquisition of X-ray diffraction patterns, the corresponding phases were determined through library scanning using the PDXL (Integrated Powder X-ray Diffraction Software) software. Microhardness measurements were performed using an EMCOTEST DuraScan 70 G5 device, employing the Vickers hardness method with a diamond pyramid tip under 50 gf load and 15 s dwell times. Hardness measurements of coating layers were conducted by moving from the cross-sectional surface towards the interior, leaving a minimum distance of twice the indentation size between traces. At least 5 hardness values were obtained for each coating layer, and their averages were considered as the hardness value for that specific layer.

2.5 Wear Test

Untreated 1.337 PMS and samples coated with three different methods were subjected to wear tests using a ball-on-disk type adhesive wear testing machine. The wear tests were performed at room temperature and 500 °C, applying a 10 N load, 250 mm/s speed, and against a 6.3 mm diameter Al_2O_3 ball. In a study evaluating the wear behavior of hardfacing alloys, Al_2O_3 balls with a hardness value of 2720 HV0.05 were used in experiments, highlighting their robustness (Kılınc et al., 2022). All Wear Test parameters are given in Table 3. To ensure the accuracy of the results, each test was repeated three times, and volume and friction coefficients were measured. The data obtained from these tests were organized in Excel, taking the arithmetic average of the results. After the wear tests, the width and depth of the circular wear tracks were measured at 0°, 90°, 270°, and 360° for each sample using an optical microscope and a 2D profilometer. The shape of the resulting wear track was observed to be semi-elliptical and was calculated in Excel using the formula below, based on previous studies (Gunen et al., 2022b; Gunen ve Ergin 2023).

Table 3. Wear test parameters

Wear Test Parameters	
Temperature	24ºC, 500 ºC
Load	10 N
Speed	250 mm/s
Test ball	6.3 mm diameter Al_2O_3

$$L = 2\pi r \quad (1)$$

$$V = 0.25\pi WD \quad (2)$$

$$Wr = V/FS \quad (3)$$

Where, L represents the length of the wear track (mm), V stands for the wear track volume (mm^3), r denotes the radius of the wear track (mm), W is the average width of the wear track (μm), D represents the average depth of the wear track (μm), F corresponds to the applied load (N), S is the sliding distance (m), and Wr is the wear rate (mm^3/Nm) (Günen et al., 2022a).

3. RESULTS AND DISCUSSION

3.1 XRD Analyses and Microstructure

XRD analyses were conducted to determine the phase structure of the untreated PMS 1.337 sample and coated samples. The obtained XRD patterns are presented in Figure 2.

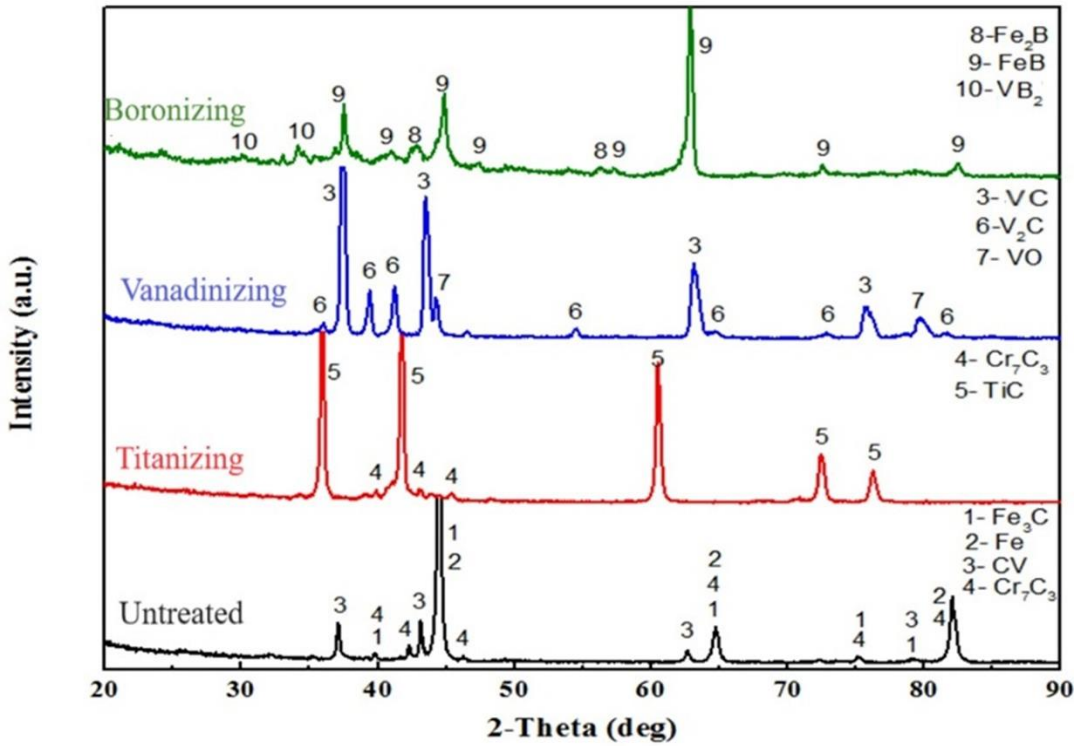

Figure 2. XRD patterns of untreated PMS 1.337 and coated samples.

As seen in Figure 2, the untreated PMS 1.3377 sample exhibits a dominant austenite peak at 44.80°, along with low levels of Fe_3C, VC, and Cr_7C_3 peaks, in accordance with the chemical composition of the PMS 1.337. In the boronized sample, the dominant phase is identified as FeB at 36.74°, 44.8°, and 63.33°, accompanied by a lower presence of Fe_2B and V_2B phases. The vanadinized sample reveals the dominance of the VC phase at 37.5°, 43.5°, 63.5°, and 76.0° along with the emergence of V_2C and VO phases. For the titanized sample, the presence of TiC phases is evident at 36°, 42.5°, 60°, 72.5°, and 76.5° degrees, alongside the detection of Cr_7C_3 phases. The obtained phase structures align with previous studies on boronizing, titanizing, and vanadinizing on steels, as reported in the literature (Şen 2004; Kurt et al. 2018; Karakaş 2020; Çakır 2022).

To validate the accuracy of the obtained phases in XRD analyses, the samples were examined using SEM, and EDS line analyses were conducted along the coating layers. SEM images taken from the cross-sectional surfaces of the coatings and EDS line analyses are presented in the range of Figure 3 to Figure 5.

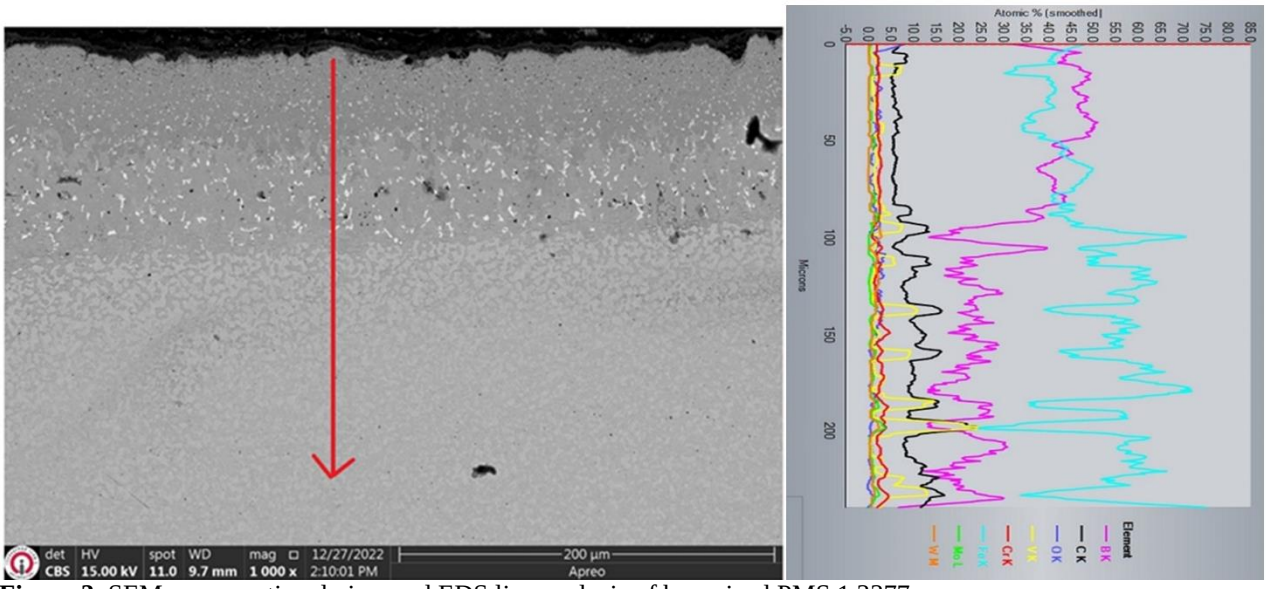

Figure 3. SEM cross-sectional view and EDS line analysis of boronized PMS 1.3377.

Upon examining the SEM microstructure image of the boride layer formed at 950°C for 2 hours using the TRD method (Figure 3), a continuous coating layer of approximately 100 µm along the surface, free from issues such as cracks and porosity, is observed. The EDS line analysis confirms that this layer is composed of Fe and B, validating its identification as a boride layer, as indicated in XRD analyses. Further analysis of the boron layer reveals a slight difference in boron content between the 0-50 µm range and the 50-100 µm range. The boron and iron ratios in the 0-50 µm range, around 50%, suggest the formation of the FeB phase in this region, consistent with XRD analyses. As the boron ratio decreases to approximately 35-40% and the iron ratio increases to around 60% in the 50-100 µm range, it indicates a decrease in diffusion from the surface towards the interior, and this region corresponds to the formation of the Fe2B phase, in accordance with XRD analyses. A transition region of approximately 20-25 µm is clearly observed both in the microstructure image and EDS line analysis beneath the 100 µm coating layer. The presence of a transition region between the coating layer and the substrate is a consequence of thermo-reactive coatings being diffusional coatings, resulting in higher adhesion between the coating and the substrate compared to coatings such as non-diffusional coatings and thermal spray coatings (Kara et al., 2016; Kurt et al., 2020; Campos-Silva et al., 2023)

Upon examining the SEM microstructure image of the sample treated with titanizing at 950°C for 2 hours using the TRD method (Figure 4), it is observed that a coating layer of approximately 10 µm has formed on the surface. This coating layer exhibits a dense and continuous uniform coating. EDS line analysis reveals that the atomic ratio of Ti in the coating layer is in the range of 60-65%, while the C content decreases from 40% to 30%. The very low presence of elements other than Ti and C in the coating layer indicates that the Cr_7C_3 phase determined in XRD analyses originates from the substrate material rather than the coating layer, and the coating layer consists solely of TiC. EDS line analysis shows that an extremely thin (~2 µm) transition region has formed between the coating layer and the matrix (Zakharov et al., 1989; Kasprzycka, E. 2015), and beneath this region, it exhibits a chemical composition consistent with the chemical composition of the 1.3377 powder metallurgy steel.

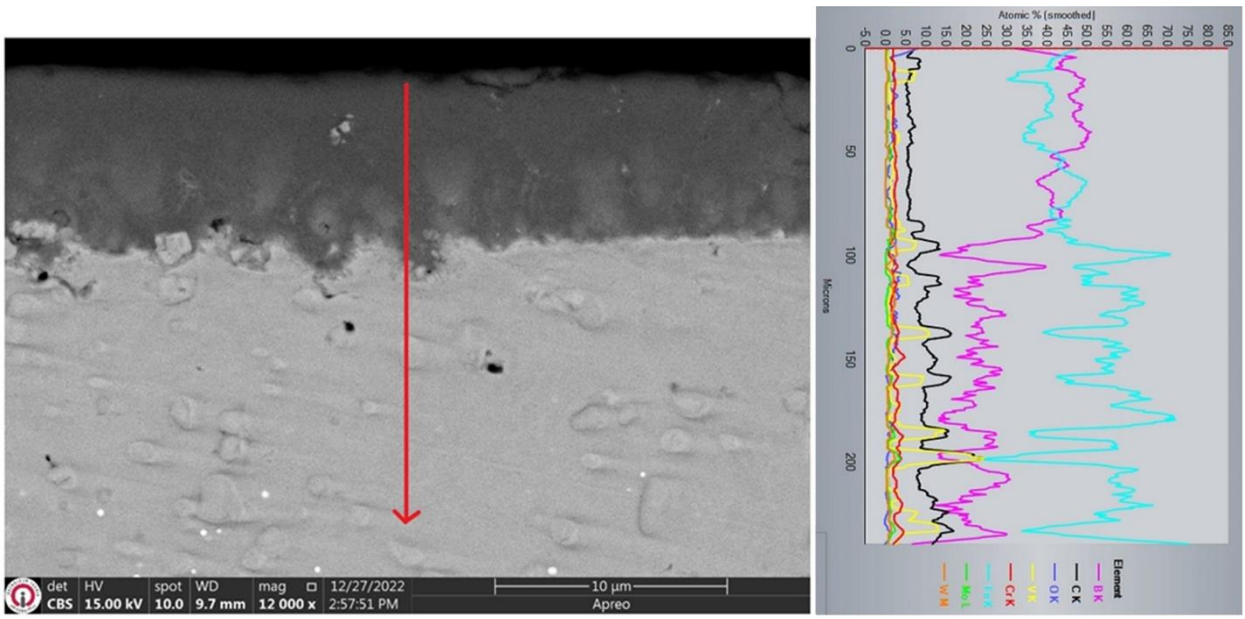

Figure 4. SEM cross-sectional view and EDS line analysis of titanized PMS 1.3377.

Considering the SEM microstructure image of the sample treated with vanadinizing at 950°C for 2 hours using the TRD method (Figure 5), it is observed that the coating layer is thicker compared to nitriding but thinner compared to boronizing, with a thickness of approximately 14-15 µm. Analysis of the coating layer through SEM microstructure images and EDS line profile indicates the presence of non-homogeneous regions, unlike boronizing and titanizing. In EDS line analyses, it is determined that these non-homogeneous regions consist of V and C, in addition to Fe and O_2. This may be attributed to insufficient oxidation prevention measures for vanadium nitriding due to the implementation of the coating process in an open-air environment (Çakır 2022).

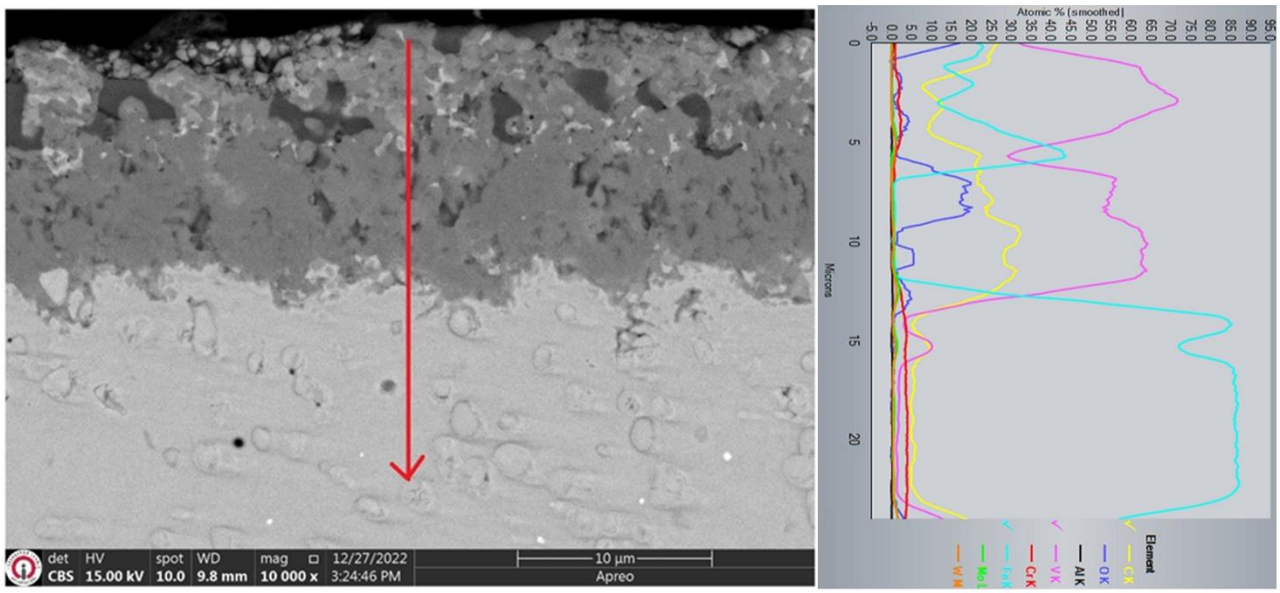

Figure 5. SEM cross-sectional view and EDS line analysis of vanadinized PMS 1.3377.

The coatings applied to PMS 1.3377 are aimed at enhancing wear resistance by improving the surface hardness of this alloy. The microhardness values of the coatings were determined using the Vickers method, and the obtained data are presented in Table 4.

Table 4. Microhardness values obtained based on TRD methods.

Sample	Coating thickness (µm)	Micro-hardness ($HV_{0.1}$)
Boronizing	98 ± 2.1	2566± 125
Titanizing	11 ±0.5	2037± 104
Vanadinizing	13.5 ±0.6	1800± 197
PMS 1.3377	-	334±30

Upon examining Table 3, it is observed that the coating layer thicknesses are approximately 98±2.1 µm for boronizing, 11±0.5 µm for tetanizing and finally, 13.5±0.5 µm for vanadinizing coating. Analyzing the microhardness values reveals measurements of 2566 HV0.1 for boronizing, 2037 HV0.1 for TiC layer, and 1800 HV0.1 for VC. When evaluating the microhardness values, it is noted that the hardness value of 2566 HV identified in boronizing is higher than the literature-specified hardness values for FeB 1900-2100 HV and Fe_2B 1650-1850 HV (Kayali et al., 2010; Campos-silva et al., 2023). This may be attributed to the V_2B phase formed within the two boride layers. On the other hand, the detection of TiC phase, specified as 3200 HV in the literature (Kurt et al. 2018), and VC phase, specified as 2950 HV (Günen et al. 2020), at lower hardness values in titanium coating can be attributed to the formation of Cr7C3 in titanium coating and V2C and VO phases in vanadium coating, which are present in low amounts in the coating content.

3.2 Wear Behaviors

In order to gain insights into the behavior of the friction coefficient during the wear test, the friction coefficient was measured. The obtained data was processed using Excel, and graphs for room temperature and 500 °C were prepared, as presented in Figure 6.

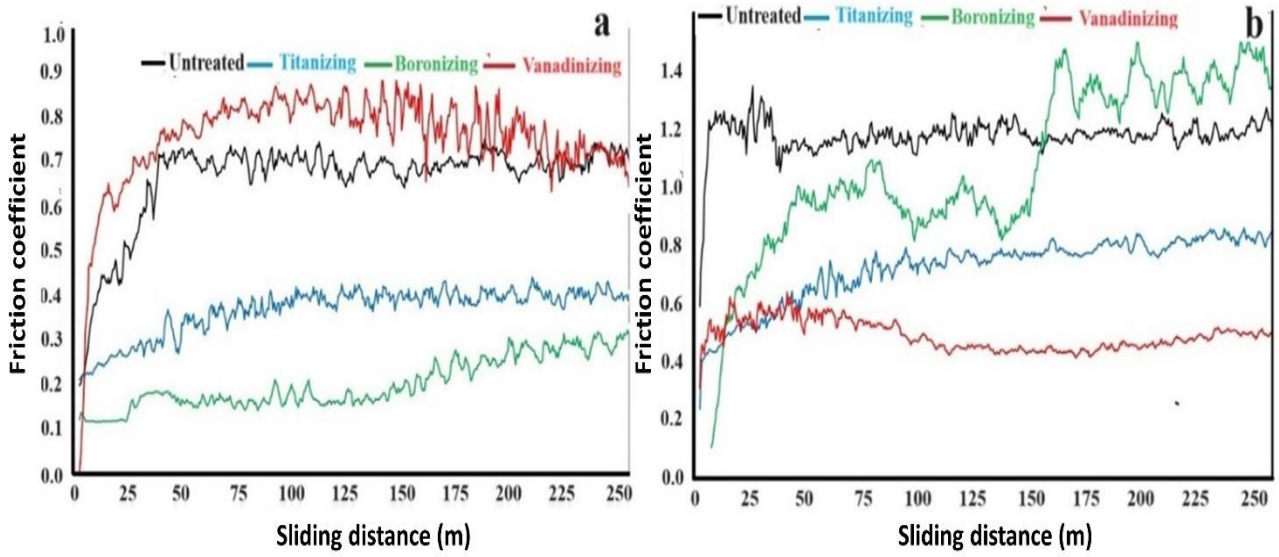

Figure 6. Friction coefficient of untreated PMS 1.337 and coated specimens at a) room temperature b) 500 °C.

Considering Figure 6a, it is observed that the 1.3377 PMS specimen exhibits a rapid increase to the level of 0.7 within the first 20 m, followed by a zigzag trend in the range of 0.65-0.75 until the end of the test. In Figure 6a, the titanized specimen shows a slight increase in the friction coefficient, starting from 0.2 and ending at the level of 0.35 at the end of the test. Therefore, it can be stated that the titanized specimen exhibits a significantly lower friction coefficient compared to the untreated specimen. Similarly, the boronized specimen shows a lower friction trend compared to the titanium-

coated specimen. However, when examining the friction coefficient graph of the vanadinized specimen, it is observed that there are periods (25-200 m) where the friction coefficient is higher than the untreated specimen, and it eventually concludes at the same level as the untreated specimen at the end of the test. Considering the overall friction coefficients of room temperature wear testing, it can be concluded that boride and titanium coatings exhibit lower friction coefficients compared to the untreated specimen. However, the higher friction coefficient observed in vanadium coating suggests that hardness values have a positive effect on reducing friction (Kato 200; Gutierrez-Noda et al., 2019; Türkmen and Yalamaç 2021). Nevertheless, in the case of coating layer inhomogeneity, some regions may wear out more quickly, leading to an increase in friction coefficients due to the abrasive effect of the worn surfaces.

From the wear tests conducted at 500 °C, the friction coefficient graphs (Figure 6b) reveal that the friction coefficient of untreated PMS 1.3377 rapidly increases in the 0-25 m range, slightly decreases in the 25-50 m range, and shows a fluctuating pattern of increase and decrease between 50-160 m, continuing with horizontal zigzag movements until the completion of the test. The friction coefficient of untreated PMS 1.3377 starts at 0.6 and peaks and reach to 1.38. Analyzing the friction coefficient graph of the titanized sample at 500 °C shows a slight increase similar to room temperature but with the friction coefficient approximately doubling. In this case, the friction coefficient starts at 0.2 and reaches maximum levels around 0.8. For the boronized sample, a continuous increase is observed in the 0-75 m range, followed by a decrease up to 150 m, a rapid increase between 150-175 m, and subsequent fluctuations of increases and decreases until the end of the test. Examining the entire test, the friction coefficient starts at 0.1 and reaches up to 1.5. This is believed to result from the sintered hard boride layer undergoing oxidation at high temperatures, acting as an abrasive between the abrasive ball and the substrate material (Zhang et al., 2023). Finally, for the vanadinized sample, the friction coefficient starts at 0-25 m, reaches around 0.5 in the 25-50 m range, experiences a slight increase from 75-125 m, and exhibits a mild increase from 175 m until the end of the test. Therefore, in high-temperature wear tests, the coatings undergo faster oxidation compared to room temperature, leading to the abrasive function of broken particles in hard coatings. This complex behavior is attributed to the formation, breakage, and regeneration of oxide layers by the complex boride and carbide phases within the structure. As long as the formed oxide layer remains unbroken, it acts as a lubricating effect, reducing friction coefficients. However, when the oxide layer breaks, the hard oxides act as abrasives, resulting in an increase in friction coefficient values (Taktak et al., 2008; Carlos et al., 2017; Günen ve Ergin 2023).

An increase in friction coefficients generally implies an escalation in wear volume losses. The wear volume losses of the samples subjected to wear tests at room temperature and 500 °C are illustrated in Figure 7.

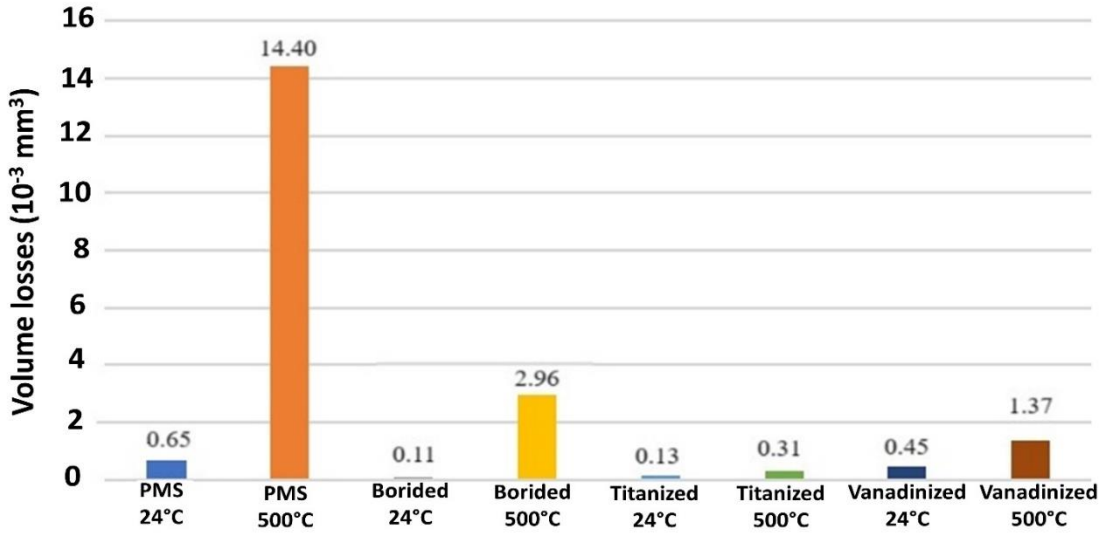

Figure 7. Wear volume losses of untreated PMS 1.337 and coatings at room temperature and 500 °C.

When examining Figure 7, it is evident that both temperature and coating methods have a significant impact on wear volume losses. Specifically, the untreated sample exhibited a wear volume loss of 0.653 × 10-3 mm³ at room temperature. However, at 500 °C, this sample experienced a 22.05-fold increase in wear compared to room temperature, resulting in a wear volume loss of 14.40 × 10-3 mm³. Furthermore, all of the coatings demonstrated lower wear volume losses compared to the untreated sample. In descending order of wear resistance relative to the untreated sample, these are ranked as boride coatings (5.88 times), TiC coating (5.14 times), and VC (1.44 times). The correlation between the wear resistance of the samples at room temperature and their surface hardness values, as observed in the literature, underscores the relationship between wear resistance and hardness. A harder surface requires higher force for plastic deformation. Examining the wear volume losses at high temperatures, a notable observation is that all coating samples experienced lower wear volume losses compared to the untreated sample, mirroring the trend observed at room temperature. However, upon closer examination of the wear volume losses at 500 °C of coatings, it is observed that the highest wear volume loss occurred in the boronized sample, which had the lowest wear volume loss at room temperature. This phenomenon may be attributed to the dual-layered coating structure of the boride layer, as depicted in the SEM image in Figure 2. The different thermal expansion coefficients of FeB and Fe_2B within the boride layer could lead to varied responses to temperature effects, resulting in distinct reactions of the phases during high-temperature wear (Kulka et al., 2017; Hamamcı et al., 2024). On the other hand, considering the volume losses in 500 °C wear tests, it is determined that the TiC coated sample exhibited the best wear resistance.

In order to identify wear mechanisms, SEM images of wear tracks were taken, and EDS analyses were conducted at relevant locations. In pictures 8 to 15, SEM images numbered I should be magnified at X40, images numbered II should be magnified at X200, and images numbered III should be magnified at X2000.

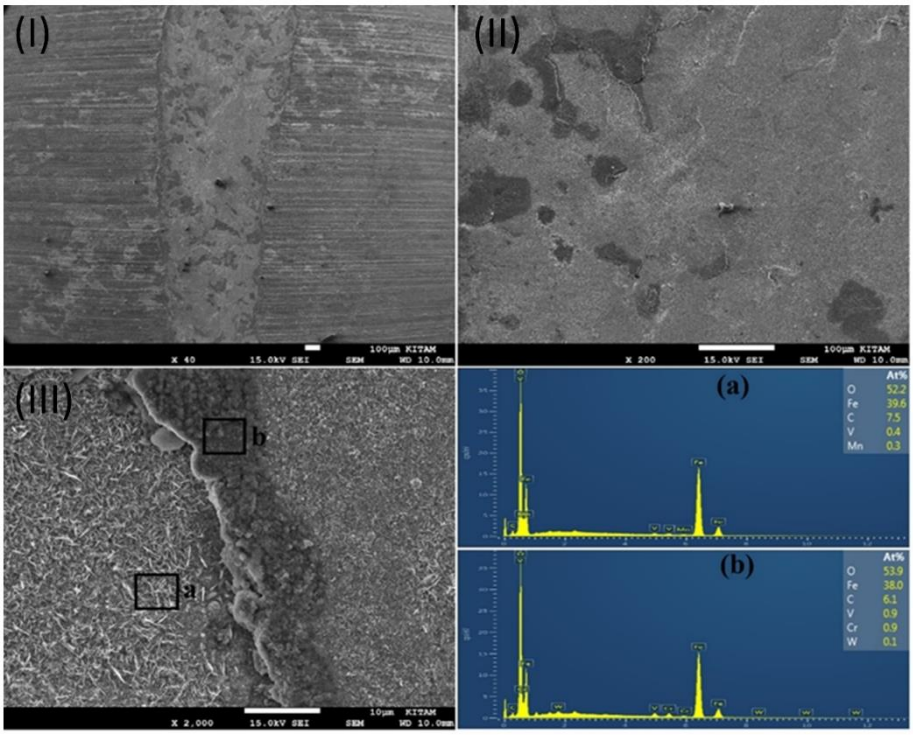

Figure 8. SEM view and EDS analysis taken from the wear scar of the untreated 1.3377 PMS worn at room temperature.

When Figure 8 is examined, it can be seen that delamination and oxidation type wear mechanisms are the dominant wear mechanisms in the sample. Delamination wear mechanism is defined as the formation of cracks beneath the surface as a result of the stresses generated under the surface by the load applied to a material exceeding the tensile strength of the material (Zhao et al. 2010; Wang et al. 2010; Demir et al. 2020), and these cracks progress towards the surface and peeling off the surface particles from the surface, causing an appearance similar to casing. In these regions where the flaking occurs, oxide layers often form in the areas of the flacked. As a matter of fact, the fact that around 50% oxygen was detected in the EDS analyzes taken from the black areas on the surface of this material (Figure 8c b region) supports this point. Indeed, the EDS analyses conducted on the areas appearing black on the material's surface (Figure 8c, region b) revealed an atomic concentration of approximately 50% oxygen, supporting this observation.

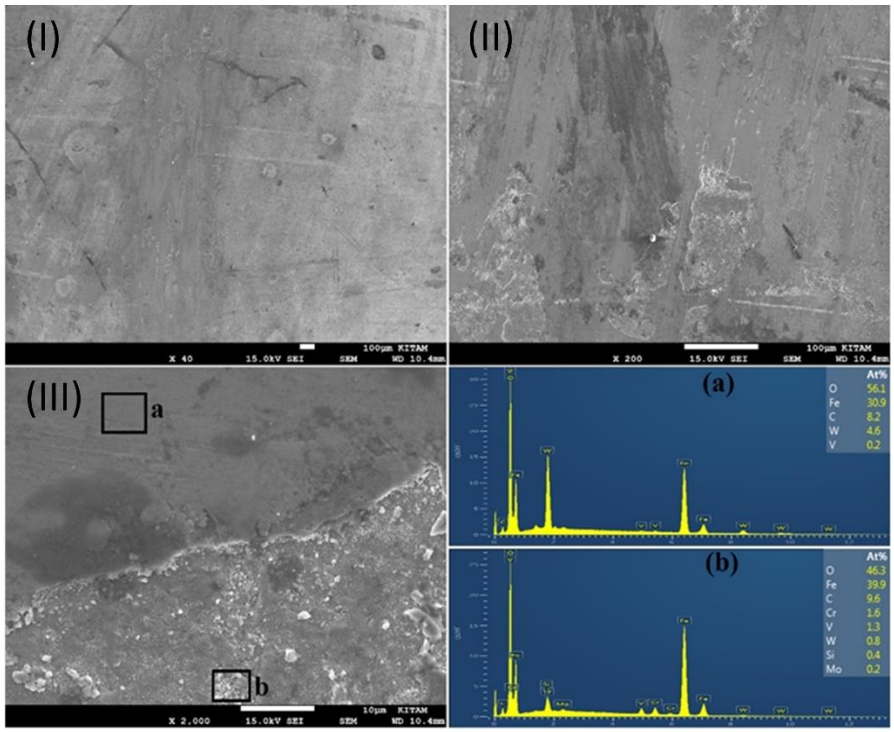

Figure 9. SEM view and EDS analysis taken from the wear scar of the untreated 1.3377 PMS worn at 500 °C.

Upon examining Figure 9, it is observed that a smoother surface has formed compared to room temperature; however, Figure 9c reveals that a portion of this surface has fractured. This condition is attributed to particles detached from the softened surface at 500 °C adhering to the surface, undergoing oxidation during the wear process due to the combined influence of temperature and ambient air, and subsequently breaking due to repeated loads. EDS analyses, detecting an oxygen concentration above 50% in this region, indicate the presence of oxidation. Therefore, the wear mechanism in this specimen is identified as adhesive-supported oxidation wear.

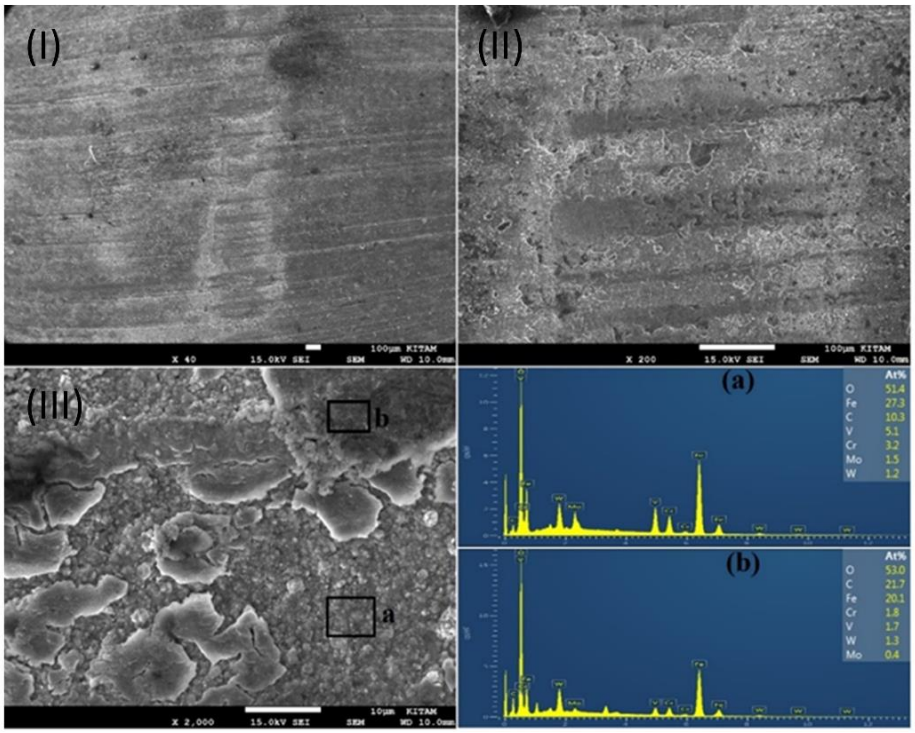

Figure 10. SEM view and EDS analysis taken from the wear scar of the borided PMS worn at room temperature.

Considering the SEM images of the worn surface of the boronized specimen at room temperature, it has been observed that the visibility of wear features on the surface is minimal. This finding supports the evidence presented in Figure 7, indicating the least wear volume losses occurring in this specimen. Upon closer inspection of the 2000X magnification image, it is understood that the wear event occurred as a result of the fracture of the boride layer due to the merging of microcracks. EDS analyses conducted on these regions revealed an atomic oxygen concentration above 50%, a consequence of the oxidation process occurring due to the wear tests being conducted in an open-air environment.

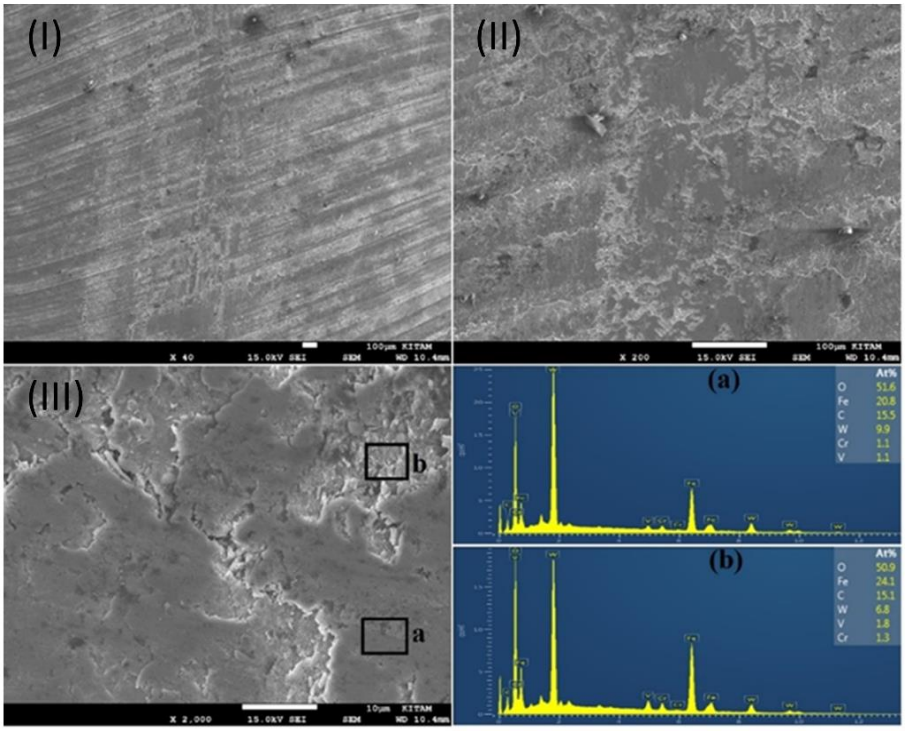

Figure 11. SEM view and EDS analysis taken from the wear scar of the borided PMS worn at 500 °C.

When examining of the SEM image of the worn surface of the boronized specimen at 500 °C, it is observed that, unlike at room temperature, there are smooth areas where material has adhered to the surface and deep delamination regions between these areas. The flat surfaces in these regions indicate that wear debris adhered (sintered) to the surface due to the 500 °C temperature and applied load, and the delamination zones suggest that these adhered debris are worn again due to repeated loads. In regions taken from the surface, an oxygen concentration above 50% is detected, indicating the occurrence of adhesion, oxidation, and delamination mechanisms in the boronized specimen during high-temperature wear testing.

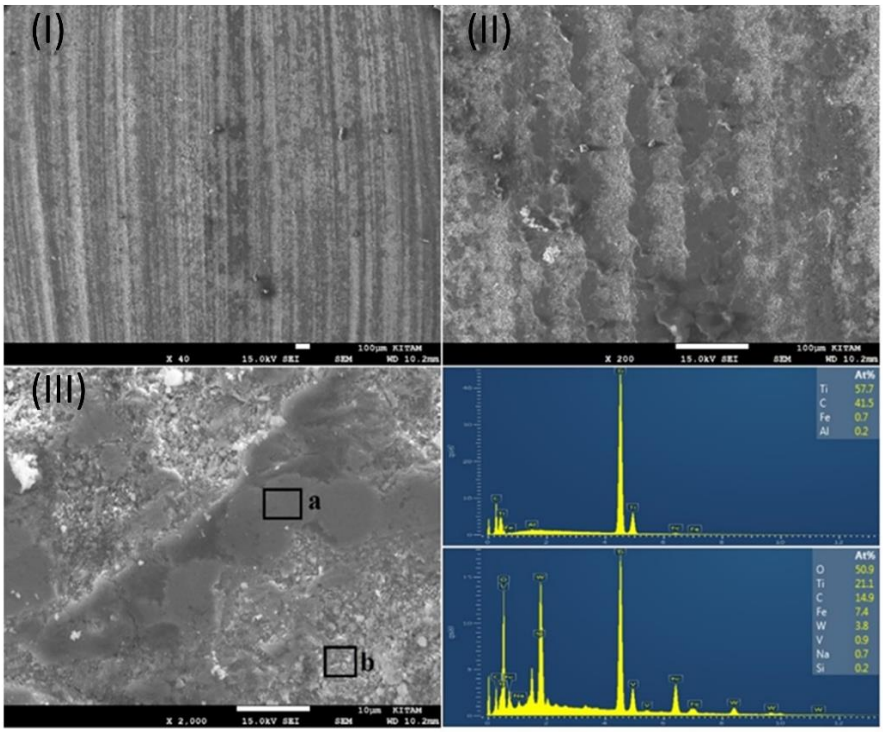

Figure 12. SEM view and EDS analysis taken from the wear scar of the titanized PMS worn at room temperature.

When examining the SEM images of the room temperature wear tracks on the titanium-coated specimen, abrasive wear marks on the surface are clearly visible. In the 200X SEM image of the specimen, these abrasive marks are observed to form channels (grooving), and according to EDS analyses of the dark areas marked as (a), they consist of unworn TiC layers. On the other hand, the white, fractured areas marked as (b) are concluded to be composed of the damaged TiC coating and the substrate material. Based on these observations, it was concluded that the oxidatively supported abrasive wear mechanism was dominant in this sample.

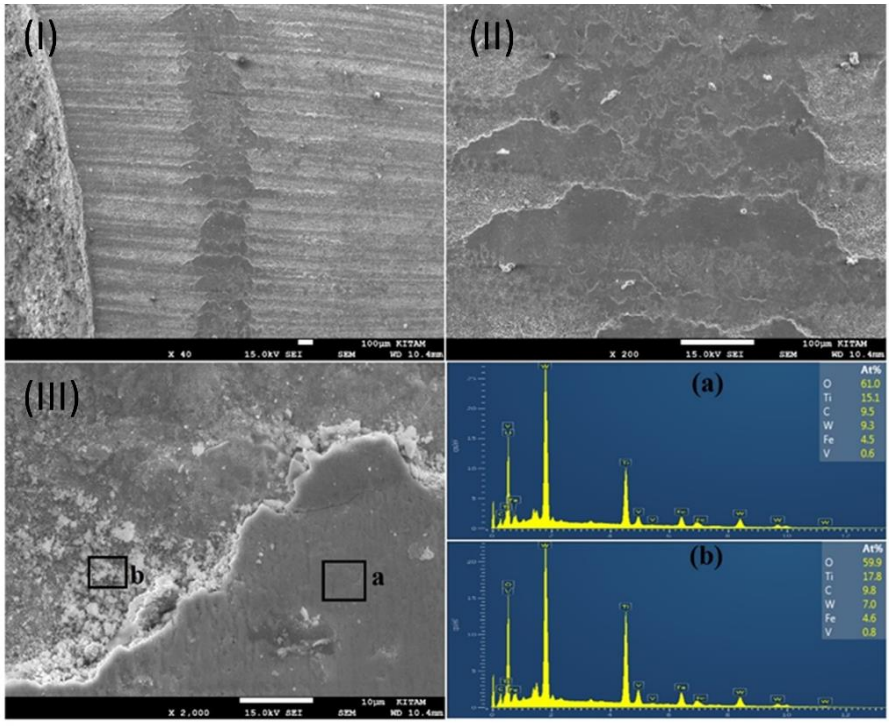

Figure 13. SEM view and EDS analysis taken from the wear scar of the titanized PMS worn at 500 °C.

Considering the SEM images of the wear tracks on the titanium-coated specimen at 500 °C, it is observed that the wear process resulted in the particles detached from the surface during wear adhering (sintering) to the surface (Günen et al. 2022b), forming a vertically oriented stripe on the horizontal specimen surface, similar to TiC coatings. In the 2000X SEM image of the specimen, it is clearly visible that these adhered regions experience fractures due to the progression of micro-cracks on the surface (Mohan et al. 2012). EDS analyses from both intact (a) and fractured (b) regions, where elements such as Ti, C, Fe, and O are closely located, strengthen the claim that the surface is composed of adhered wear debris, as mentioned above. This situation indicates that the wear mechanism at elevated temperatures occurs as an oxidative-supported adhesive wear mechanism.

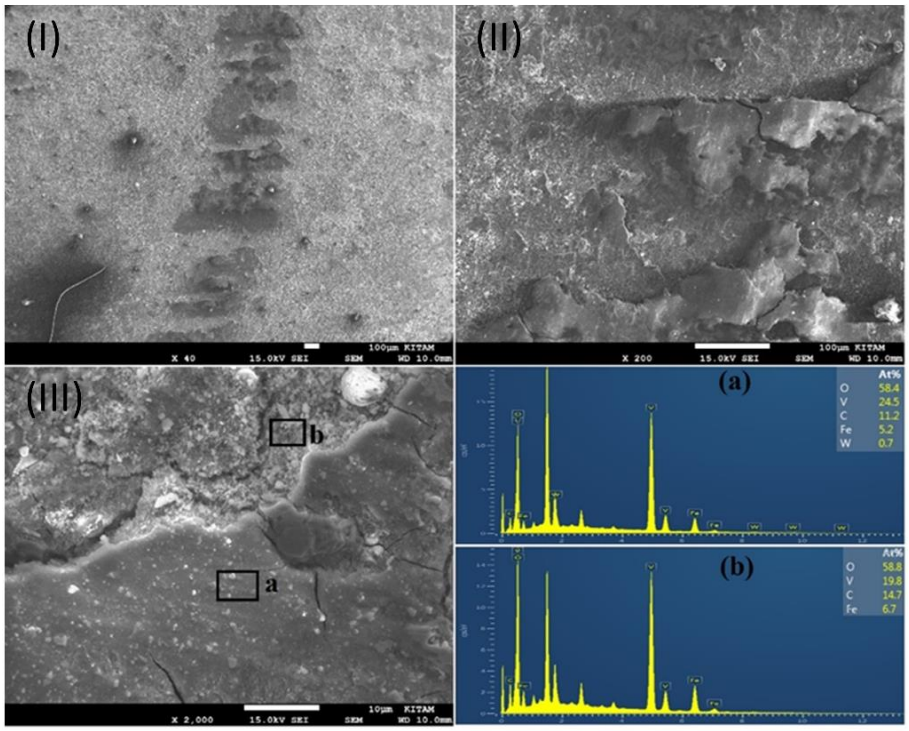

Figure 14. SEM view and EDS analysis taken from the wear scar of the vanadinized PMS worn at room temperature.

When examining Figure 14, it is observed that particles adhered to the surface, similar to the 500 °C-abraded TiC sample, also occur on the surface of the vanadium-coated specimen. This phenomenon is a consequence of the sample's susceptibility to wear due to the mentioned heterogeneity in its microstructure, making it more prone to wear and causing the wear particles to adhere to the surface due to the compression between the abrasive ball and the material. Upon closer inspection of the 2000X SEM images of the specimen, it is evident that these adhered regions harbor numerous micro-cracks, with some areas breaking due to the progression of these micro-cracks. EDS analyses from both intact (a) and fractured (b) regions, where elements such as V, C, Fe, and O are closely located, support the claim that the surface is composed of sintered wear debris, as mentioned above. Therefore, the similarity in the wear volume loss between the vanadium-coated specimen at room temperature and the titanium-coated specimen at 500 °C strengthens the aforementioned observations.

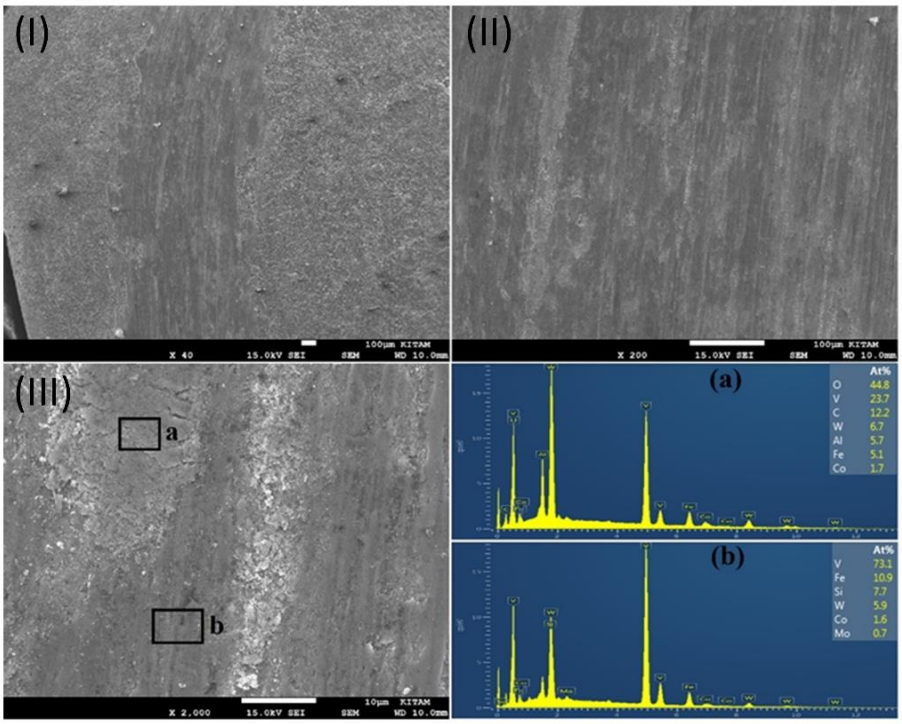

Figure 15. SEM view and EDS analysis taken from the wear scar of the vanadinized PMS worn at 500 °C.

When the wear trace SEM images of the vanadinized sample at 500 °C are examined, a much smoother wear surface is seen compared to room temperature. When the 2000X image of the sample is examined, it is seen that the flat surface actually consists of sintered wear debris and that these areas consist of gaps and cracks within themselves. EDS analyzes show that a similar wear mechanism occurs in these samples at room temperature.

4. CONCLUSION

In this study, the effects of boride and carbide coatings formed with TRD coatings on the surface of cutting edge 13377 PMS, produced by powder metallurgy method, on the microstructure and wear behavior of this alloy were studied. After the coating process, characterization studies were carried out by SEM, EDS, XRD, microhardness test, room temperature and high temperature wear tests. The results obtained are summarized below.

1- Dense, continuous and homogeneous coatings were obtained on the surface by boronizing and titanizing processes while in vanadinizing oxide formation and unhomogeneity in the coating layer detected.

2- XRD analyzes showed that the dominant phase in the coated samples was FeB for boronizing, TiC for titanizing and VC for vanadinizing. Additionally, apart from these phases, phases such as Cr_7C_3, VO, V_2B were formed in low amounts depending on the chemical composition and the applied coating method.

3- PMS 1.3377 steel, whose hardness was determined as 334 HV, was improved up to 2566 HV by boronizing, 2034 HV by titanizing and 1800 HV by vanadinizing, with the boride and carbide coatings formed by the applied coating processes.

4- The thickness of the coating layers obtained was determined as 98±2.1, 11±0.5, 13±0.6 for boronizing, titanizing and vanadinizing, respectively.

5- All coated samples showed lower mean friction coefficient values than the untreated sample at room temperature and 500 °C. This can be attributed to the high hardness values of borides and carbides and the fact that the oxides they form, such as B_2O_3, TiO_2, VO, are more stable than Fe_2O_3 and Fe_3O_4.

7- Coated samples exhibited up to 20 times higher wear resistance than untreated samples at both room temperature and 500 °C. While room temperature wear resistance is mostly related to the increase in hardness values, high temperature wear resistance is mostly related to the stability of the phase structure at high temperatures.

8- While the untreated sample was exposed to delamination and oxidation wear mechanisms at room temperature, the wear mechanism turned into adhesive and oxidation at 500 °C. On the other hand, it was determined that the wear mechanism in coated samples occurred in the form of adhesive, oxidation and delamination at both room temperature and 500 °C.

9- While the best wear resistance at room temperature was obtained in the boronized sample, the best wear resistance at 500 °C was obtained in the titanized sample. The fact that boriding shows the lowest wear resistance among samples coated at high temperatures can be attributed to the fact that the layers are exposed to different thermal expansions since they are dual-layered (FeB+Fe_2B).

10- The study demostrated that the wear resistance of PMS 1.3377, which is used in applications such as cutting tool turning, milling and drilling, can be improved by 3 different coating methods from room temperature to 500°C, but the most suitable method for this steel is titanizing.

5. ACKNOWLEDGEMENTS

This study did not benefit from any support.

6. CONFLICT OF INTEREST

Authors approve that to the best of their knowledge, there is not any conflict of interest or common interest with an institution/organization or a person that may affect the review process of the paper.

7. AUTHOR CONTRIBUTION

Erdoğan Kanca determined and managed the concept and design process of the research. Talat TURAN collected the data of the experiments related to the study and made the necessary graphic drawings. Ali Günen analyzed the SEM, EDS, XRD and microhardness data for the study and interpreted the results. All authors prepared and critically analyzed the manuscript.

8. REFERENCES

Angelo, P. C., Subramanian, R., & Ravisankar, B., Powder metallurgy: science, technology and applications. PHI Learning Pvt. Ltd., 2022.

Arai, T., The thermo-reactive deposition and diffusion process for coating steels to improve wear resistance. In Thermochemical surface engineering of steels (pp. 703-735). Woodhead Publishing, 2015.

Aras, M., Şahin, M., & Gündoğdu, Ö., Effects of sintering temperature on microstructural properties of ni1-xznxfe2o4 synthesized by powder metallurgy. Materials Science/Medziagotyra, , 28(4), 487-495, 2022. https://doi.org/10.5755/j02.ms.30204

Campos Silva, I. E., Günen, A., Serdar Karakaş, M., & Delgado Brito, A. M., The Boriding Process for Enhancing the Surface Properties of High-Temperature Metallic Materials. Coatings for High-Temperature Environments: Anti-Corrosion and Anti-Wear Applications, 221-259, 2023.

Claros, J. M., do Nascimento, E. M., & D Oliveira, A. S. C. M., Effect of the oxide film on the sliding wear behavior of a CoCrMoSi alloy hard facing coating. In 24th ABCM International Congress of Mechanical Engineering: pp. 3-8, 2017.

Çakir, M. V., A Comparative Study on Tribocorrosion Wear Behavior of Boride and Vanadium Carbide Coatings Produced by TRD on AISI D2 Steel. Protection of Metals and Physical Chemistry of Surfaces, 58(3), 562-573, 2022.

Çalıgülü, U., Durmuş, H., Akkaş, M., & Sahin, B., Microstructure and mechanical properties of ni matrix b4c reinforced functionally graded composites. Science of Sintering, 53(4), 475-484, 2021. https://doi.org/10.2298/sos2104475c

Çalık, A., Karakaş, M. S., Uçar, N., & Ünüvar, F., Boriding kinetics of pure cobalt. Metallic Materials, 52(02), 107-112, 2021. https://doi.org/10.4149/km_2014_2_107

Daicu, R., Chivu, C., & Oancea, G., A case study about acquisition of mechanically fixed cutting inserts. MATEC Web of Conferences, 137, 03004, 2017. https://doi.org/10.1051/matecconf/201713703004

Dement, T. V., Kurzina, I., Калашников, М. П., Попова, Н. А., & Karakchieva, N., Structure and phase composition of material based on vanadium alloy v-4.9ti-4.8cr and ferrite steel 17cr-12ni-fe. MATEC Web of Conferences, 243, 00019, 2018. https://doi.org/10.1051/matecconf/201824300019

Demir, M., Kanca, E., & Karahan, I. H., Characterization of electrodeposited Ni–Cr/hBN composite coatings. Journal of Alloys and Compounds, 844, 155511, 2020.

Duran, H., Özkan, D., Karaoğlanli, C., Borlama işlemi uygulanmış Inconel 718 süperalaşımın mikroyapı, aşınma ve mekanik özelliklerinin incelenmesi. Karaelmas Fen ve Mühendislik Dergisi, 11(1), 61-72, 2021. DOI:10.7212/ karaelmasfen.811408

Erden, M. A., Yaşar, N., Korkmaz, M. E., Ayvacı, B., Nimel Sworna Ross, K., & Mia, M., Investigation of microstructure, mechanical and machinability properties of Mo-added steel produced by powder metallurgy method. The International Journal of Advanced Manufacturing Technology, 114, 2811-2827, 2021.

Fang, Z. Z., Paramore, J. D., Sun, P., Chandran, K. R., Zhang, Y., Yang, X., … & Free, M. L., Powder metallurgy of titanium – past, present, and future. International Materials Reviews, 63(7), 407-459, 2017. https://doi.org/10.1080/09506608.2017.1366003

Hamamcı, M., Nair, F., Cerit, A. A., & Güneş, R., Thermal shock effects on the microstructure and mechanical properties of iron-based composites reinforced by in-situ Fe2B/FeB ceramic phases. Ceramics International, 43(1), 1584-1587.2024.

Hasçelik, A., & Aslantaş, K., Mikro Tornalama İşleminde Kesici Takım Burun Yarıçapının Kesme Kuvvetlerine Etkisi. Journal of Materials and Mechatronics: A, 2(1), 13-25, 2012.

Gevorkyan, E., Rucki, M., Sałaciński, T., Siemiątkowski, Z., Nerubatskyi, V., Kucharczyk, W., … & Nejman, M., Feasibility of cobalt-free nanostructured wc cutting inserts for machining of a tic/fe composite. Materials, 14(12), 3432, 2021. https://doi.org/10.3390/ma14123432

Ghadi, A., Ebrahimnezhad-Khaljiri, H., & Gholizadeh, R., A comprehensive review on the carbide-base coatings produced by thermo-reactive diffusion: microstructure and properties viewpoints. Journal of Alloys and Compounds, 171839, 2023.

Gökmen, U., Eslam Jamal Golzari, L., Gürgen Avşar, S., Özkan, Z., & Bilge Ocak, S., Microstructural and radioactive shielding analyses of alumix-231 and alumix-231 reinforced with b4c/sic/al2o3 particles produced through hot pressing. ACS Omega, 8(39), 35755-35767, 2023. https://doi.org/10.1021/acsomega.3c03132

Gutierrez-Noda, L., Cuao-Moreu, C. A., Perez-Acosta, O., Lorenzo-Bonet, E., Zambrano-Robledo, P., & Hernandez-Rodriguez, M. A. L., The effect of a boride diffusion layer on the tribological properties of AISI M2 steel. Wear, 426, 1667-1671, 2019.

Günen, A., Kanca, E., Demir, M., Er, Y., Sağlam, G., & Gök, M. S., Microabrasion wear behavior of fast-borided steel tooth drill bits. Tribology Transactions, 60(2), 267-275, 2016. https://doi.org/10.1080/10402004.2016.1159359

Günen, A., Kalkandelen, M., Karahan, İ. H., Kurt, B., Kanca, E., Gök, M. S., & Serdar Karakaş, M., Properties and corrosion behavior of chromium and vanadium carbide composite coatings produced on ductile cast iron by thermoreactive diffusion technique. Journal of Engineering Materials and Technology, 142(4), 041008, 2020.

Günen, A., Lindner, T., Karakaş, M. S., Kanca, E., Töberling, G., Vogt, S., ... & Lampke, T., Effect of the boriding environment on the wear response of laser-clad AlCoCrFeNi high entropy alloy coatings. Surface and Coatings Technology, 447, 128830, 2022.

Günen, A., Soylu, B., & Karakaş, Ö., Titanium carbide coating to improve surface characteristic, wear and corrosion resistance of spheroidal graphite cast irons. Surface and Coatings Technology, 437, 128280, 2022.

Günen, A., Bölükbaşı, Ö. S., Özgürlük, Y., Özkan, D., Odabaş, O., & Somunkıran, İ., Effect of cr addition on properties and tribological behavior at elevated temperature of boride layers grown on borosintered powder metallurgy alloys. Metals and Materials International, 29(3), 748-766, 2023.

Günen, A., & Ergin, Ö., A comparative study on characterization and high-temperature wear behaviors of thermochemical coatings applied to cobalt-based Haynes 25 superalloys. Coatings, 13(7), 1272, 2023.

Gürbüz, H., Şeker, U., & Kafkas, F., Effects of cutting tool forms on the surface integrity in turning of AISI 316L stainless steel. Journal of the Faculty of Engineering and Architecture of Gazi University, 35(1), 225-240, 2020.

Kara, R., Çolak, F., & Kayali, Y., Investigation of wear and adhesion behaviors of borided steels. Transactions of the Indian Institute of Metals, 69, 1169-1177, 2016.

Karakaş, M. S., Tribocorrosion behavior of surface-modified AISI D2 steel. Surface and Coatings Technology, 394, 125884, 2020.

Kasprzycka, E., Corrosion resistant layers produced in vacuum titanizing process on a low carbon steel surface coated electrolytically with cobalt. Solid State Phenomena, 223, 110-118, 2015.

Kato, K., Wear in relation to friction—a review. wear, 241(2), 151-157, 2000.

Kayali, Y., Taktak, S., Ulu, S., & Yalcin, Y., Investigation of mechanical properties of boro-tempered ductile iron. Materials & Design, 31(4), 1799-1803, 2010.

Kayalı, Y., & Yalçın, Y., Borlanmış AISI 316 L Paslanmaz Çeliğin Difüzyon Kinetiğinin İncelenmesi. Journal of Materials and Mechatronics: A, 1(1), 12-21, 2020.

Khan, M. A. and Gupta, K., A study on machinability of nickel based superalloy using micro-textured tungsten carbide cutting tools. Materials Research Express, 7(1), 016537, 2020. https://doi.org/10.1088/2053-1591/ab61bf.

Kılınç, B., Kocaman, E., Şen, Ş., & Şen, U., Effect of titanium content on the microstructure and wear behavior of fe(13-x)tixb7 (x=0-5) hardfacing alloy. Journal of Mining and Metallurgy, Section B: Metallurgy, 58(1), 29-41, 2022. https://doi.org/10.2298/jmmb210430047k

König, W., Komanduri, R., Toenshoff, H. K., & Ackershott, G., Machining of hard materials. CIRP annals, 33(2), 417-427, 1984.

Kulka, M., Makuch, N., & Piasecki, A., Nanomechanical characterization and fracture toughness of FeB and Fe2B iron borides produced by gas boriding of Armco iron. Surface and Coatings Technology, 325, 515-532, 2017.

Kurt, B., Günen, A., Kanca, Y., Koç, V., Gök, M. S., Kırar, E., & Askerov, K., Properties and tribologic behavior of titanium carbide coatings on AISI D2 steel deposited by thermoreactive diffusion. Jom, 70, 2650-2659, 2018.

Kurt, B., Özdoğan, L., Güney, B., Bölükbaşı, Ö. S., & Günen, A., Characterization and wear behavior of TiBC coatings formed by thermo-reactive diffusion technique on AISI D6 steel. Surface and Coatings Technology, 385, 125332, 2020.

Liu, S., Huang, P., Sun, X., Zeng, W., Zhang, J., & Zu, G., Fatigue of an aluminum foam sandwich formed by powder metallurgy. Materials, 16(3), 1226, 2023. https://doi.org/10.3390/ma16031226

Mathivanan, A., Sudeshkumar, M. P., Radhika, R., Ezilarasan, C., Raju, G. U., & Jayaseelan, V., Finite element simulation and regression modeling of machining attributes on turning aisi 304 stainless steel. Manufacturing Review, 8, 24, 2021. https://doi.org/10.1051/mfreview/2021022

Mohan, N., Natarajan, S., & KumareshBabu, S. P., The role of synthetic and natural fillers on three-body abrasive wear behaviour of glass fabric–epoxy hybrid composites. Journal of applied polymer science, 124(1), 484-494, 2012.

Nayak, K. C., Rane, K., Date, P. P., & Srivatsan, T. S., Synthesis of an aluminum alloy metal matrix composite using powder metallurgy: role of sintering parameters. Applied Sciences, 12(17), 8843, 2022. https://doi.org/10.3390/app12178843

Pashechko, M. I., Dziedzic, K., & Jóźwik, J., Analysis of wear resistance of borided steel c45. Materials, 13(23), 5529, 2020. https://doi.org/10.3390/ma13235529

Rizzo, A., Goel, S., Luisa Grilli, M., Iglesias, R., Jaworska, L., Lapkovskis, V., ... & Valerini, D., The critical raw materials in cutting tools for machining applications: A review. Materials, 13(6), 1377, 2020.

Sathish, T., Mohanavel, V., Karthick, A., Arunkumar, M., Ravichandran, M., & Rajkumar, S., Study on compaction and machinability of silicon nitride (si3n4) reinforced copper alloy composite through p/m route. International Journal of Polymer Science, 1-10, 2021. https://doi.org/10.1155/2021/7491679

Somunkıran, İ., Çelik, E., Tunç., B & Güneş, Ç., Toz Metalurjisi Yöntemiyle Üretilen Fe Esaslı Fe-Ni-Cu Elmas Kesici Takımında Co'ın Etkisi. Journal of Materials and Mechatronics: A, 3(2), 194-205, 2022.

Şap, E., Usca, Ü. A., Gupta, M. K., Kuntoğlu, M., Sarıkaya, M., Pimenov, D. Y., … & Mia, M., Parametric optimization for improving the machining process of cu/mo-sicp composites produced by powder metallurgy. Materials, 14(8), 1921, 2021. https://doi.org/10.3390/ma14081921

Şen, U., Thermo-reactive diffusion vanadium nitride coatings on AISI 1020 steel. Key Engineering Materials, 264, 577-580, 2004.

Taktak, S., Ulker, S., & Gunes, I., High temperature wear and friction properties of duplex surface treated bearing steels. Surface and Coatings Technology, 202(14), 3367-3377, 2008.

Turgut, S., & Günen, A., Mechanical properties and corrosion resistance of borosintered distaloy steels. Journal of Materials Engineering and Performance, 29, 6997-7010, 2020.

Türkmen, İ., & Yalamaç, E., Effect of alternative boronizing mixtures on boride layer and tribological behaviour of boronized SAE 1020 steel. Metals and Materials International, 1-15, 2021.

Vijaya Kumar, P., & Velmurugan, C., Surface Treatments and Surface Modification Techniques for 3D Built Materials. Cham: Springer International Publishing. In Innovations in Additive Manufacturing: pp. 189-220, 2022.

Wang, S. Q., Wei, M. X., Wang, F., & Zhao, Y. T., Transition of elevated-temperature wear mechanisms and the oxidative delamination wear in hot-working die steels. Tribology International, 43(3), 577-584, 2010.

Zakharov, B. V., Minkevich, A. N., Pikunov, D. V., Toné, É. R., & Argasova, E. D., Role of the phase composition of tungsten containing hard alloys in the formation of a layer of titanium carbide in gas titanizing. Soviet Powder Metallurgy and Metal Ceramics, 28(7), 574-578, 1989.

Zhao, Y. T., Wang, S. Q., Yang, Z. R., & Wei, M. X., A new delamination pattern in elevated-temperature oxidative wear. Journal of materials science, 45, 227-232, 2010.